Research on Engineering Structures & Materials
www.jresm.org
Research Group

Research Article

Structural behavior of composite hollow steel-concrete double corbels

Ruqaya Saeed Mankhi [*,a], Nasser Hakeem Tu'ma [b]

Civil Engineering Department, University of Misan, Misan, Iraq

Article Info

Article History:

Received 10 Aug 2026

Accepted 17 Sep 2026

Keywords:

Double corbel;
Structural behavior;
Composite steel-concrete;
Hollow steel section

Abstract

This study investigates the structural performance of reinforced concrete double corbels strengthened using hollow steel sections as an innovative composite strengthening technique. Six corbel specimens with a constant shear span-to-depth ratio (a/d = 0.2) were experimentally tested under monotonic loading until failure. One specimen served as a control, while the remaining specimens were strengthened using different hollow steel section configurations in the tie region, strut region, or both. The effects of concrete compressive strength and strengthening configuration were evaluated in terms of cracking load, ultimate load capacity, stiffness, toughness, ductility, and failure mode. The suggested strengthening method considerably enhanced the corbels' structural performance, according to the results, with ultimate load capacity increases ranging from 58.6% to 152.6%. Strengthening the strut region provided the highest improvement in load-carrying capacity and stiffness, while strengthening the tie region enhanced tensile resistance and delayed crack propagation. Combined strengthening produced balanced structural behavior with improved stiffness, toughness, and crack control. Augmenting concrete compressive strength improved stiffness and ultimate load capacity, although it diminished ductility, resulting in a more brittle response. Overall, hollow steel sections proved to be an effective strengthening technique for improving the behavior and load resistance of reinforced concrete double corbels.

© 2026 MIM Research Group. All rights reserved.

1. Introduction

In reinforced concrete (RC), corbels are short cantilevers that extend from walls or columns and have a low ratio of shear span to effective depth (a/d). ACI 318-19 [1] limits the value of a/d for corbels to less than 2; however, Mattock et al. [2] classified cantilevers with an a/d ratio of less than or equal to 1 as corbels. Corbels are designed to withstand enormous loads from cranes in heavy-duty manufacturing workshops, precast buildings, and bridges, as well as horizontal forces generated by temperature changes, creep, or restricted shrinkage [3–5]. The RC corbel element is primarily controlled by shear rather than moment and experiences a high concentration of tensile stress, known as a disturbed region. Consequently, the strut-tie model is often used to analyze the mechanism of corbel strength, with tensioned regions modeled as tie reinforcement and the compressive zone modeled as a concrete strut. Corbels with an a/d ratio of less than one has been studied using shear friction. The failure path is the route where structural elements dissipate the least energy. Causes of failure include shearing, tension tie yielding, compression strut splitting or crushing, and shearing failure beneath a loading plate or localized bearing [6, 7]. In certain instances, such as alterations in usage, design flaws, or degradation from inclement weather, the corbel needs reinforcement or enhancement [8].

*Corresponding author: st_chem20242@uomisan.edu.iq
[a]orcid.org/0009-0006-4632-1565; [b]orcid.org/0000-0003-1956-8539
DOI: http://dx.doi.org/10.17515/resm2026-2145ic0810rs

Earlier research on corbel strengthening employed three main approaches: post-tensioned anchored bars, external strengthening with steel plates, and exterior reinforcement with FRP composites [8,9]. Heidayet et al. [10] found that after fixing multiple damaged RC corbels with external plates, the repaired corbels' strength ratio varied between 0.7 and 1.5. Compared to other wrapping configurations, Ozden and Atalay [11] found that adding glass fiber-reinforced polymer sheets to reinforced concrete beams at a 45-degree angle had a greater effect. The improvement ranged from 40% to 200%, depending on the characteristics of the FRP layers, the (a/d) ratio, and the reinforcement ratio. El-Maaddawy and El-Sayed [12] found that CFRP sheets provided a strength gain of between 21% and 40%. Mohammed and Hassan [13] discovered that assessing CFRP-wrapped high-strength concrete corbels enhanced their load capacity by 28.3%. Ivanova and Assih [14] investigated the use of carbon fiber textiles to strengthen RCCs, achieving a failure tensile strength of over 1.82. They also evaluated the static and dynamic response of RCC reinforced with carbon fibers; stiffness increased by less than one-third, but the ultimate load doubled [15]. Urban and Krawczyk [16] proposed using post-installed threaded rods for additional support. Mohammad and AlShamaa [17] studied how Near Surface Installed (NSM) CFRP strips enhance the condition of reacting powder concrete brackets, achieving an average gain of 15%. Al-Kamaki et al. [18] used CFRP textiles to analyze the behavior of externally reinforced RCCs, finding that diagonal reinforcement increased final strength by 27%. The experimental reaction of high-strength self-consolidating reinforced concrete (RCC) with near-surface-mounted (NSM) steel bars was evaluated by Shakir and Kamonna [19] investigated four different configurations for placing reinforcing bars. For a/d ratios of 0.85 and 1.25, the maximum improvements in failure load were 57% and 41%, respectively. Braidi et al. [20] examined the performance of hollow steel-concrete composite columns exposed to unconventional tensile pressures via an experimental program comprising seven laboratory specimens. The findings indicated that incorporating a hollow steel segment within the column enhanced the tensile strength by as much as 17% relative to traditional columns. The research indicated that maximum tensile resistance was attained when the loading eccentricity approached the balanced eccentricity (±15%).

Despite the extensive investigation of RC corbel strengthening using external steel plates, FRP systems, NSM reinforcement, and post-installed steel bars, the use of embedded hollow steel sections (HSS) as an internal strengthening component for RC corbels has received limited experimental attention. The proposed technique differs from conventional steel-based, externally bonded, and steel–concrete composite strengthening systems by embedding HSS within the concrete body and strategically positioning them within the principal strut and tie regions identified by the strut-and-tie model (STM). Thus, rather than relying primarily on external reinforcement or surface-bonded strengthening, the proposed system integrates the HSS directly into the internal load-transfer mechanism of the corbel. This configuration is intended to enhance the load-transfer capacity of the principal strut and tie regions while maintaining the integrity of the external concrete surfaces. The present study experimentally evaluates the structural response of RC corbels strengthened using different HSS configurations under monotonic loading, with emphasis on load-carrying capacity, deformation, stiffness, toughness, crack propagation, and failure modes.

2. Experimental Work

2.1 Specimen Description

This research included the examination of six reinforced concrete corbels, all with identical dimensions and a constant shear span-to-depth ratio (a/d) of 0.2. Each corbel underwent testing with a uniform approach, implementing a single-point loading configuration. One specimen, along with several as controls (D-C-F30-0.2), was cast with normal-strength concrete (30 MPa) without any external reinforcement. The remaining five corbels were reinforced with hollow steel sections (HSS) in different configurations. In the first corbel, a 50×50 mm HSS was placed in the tie region (D-P-T-F30-0.2) to improve tensile strength. The second corbel was reinforced in the inclined strut region (D-P-SF30-0.2). The third and fourth corbels were reinforced in both the tie and strut regions (horizontal and inclined) (D-P-TSS-F25-0.2, D-P-TSS-F35-0.2, D-P-TSS-F30-0.2) using concrete strengths of 25 MPa and 35 MPa, respectively, to examine the effect of concrete strength

on structural behavior. The sixth corbel was reinforced with a double hollow steel section (D-P-2TSS-F30-0.2) measuring 20×20 mm, applied in both the tie and strut regions (horizontal and inclined) as shown in Figure 1.

2.3 Materials

This investigation utilized ordinary Portland cement (Crista) in accordance with IQS No. 5/2019 [21]. Natural sand from the Basra Governorate, with a maximum particle size of 4.75 mm, was utilized as fine aggregate, and crushed gravel with a maximum size of 10 mm was employed as coarse aggregate. Both aggregates satisfied the requirements of IQ. S45/1984 [22]. The sieve analysis results are presented in Tables 1 and 2.

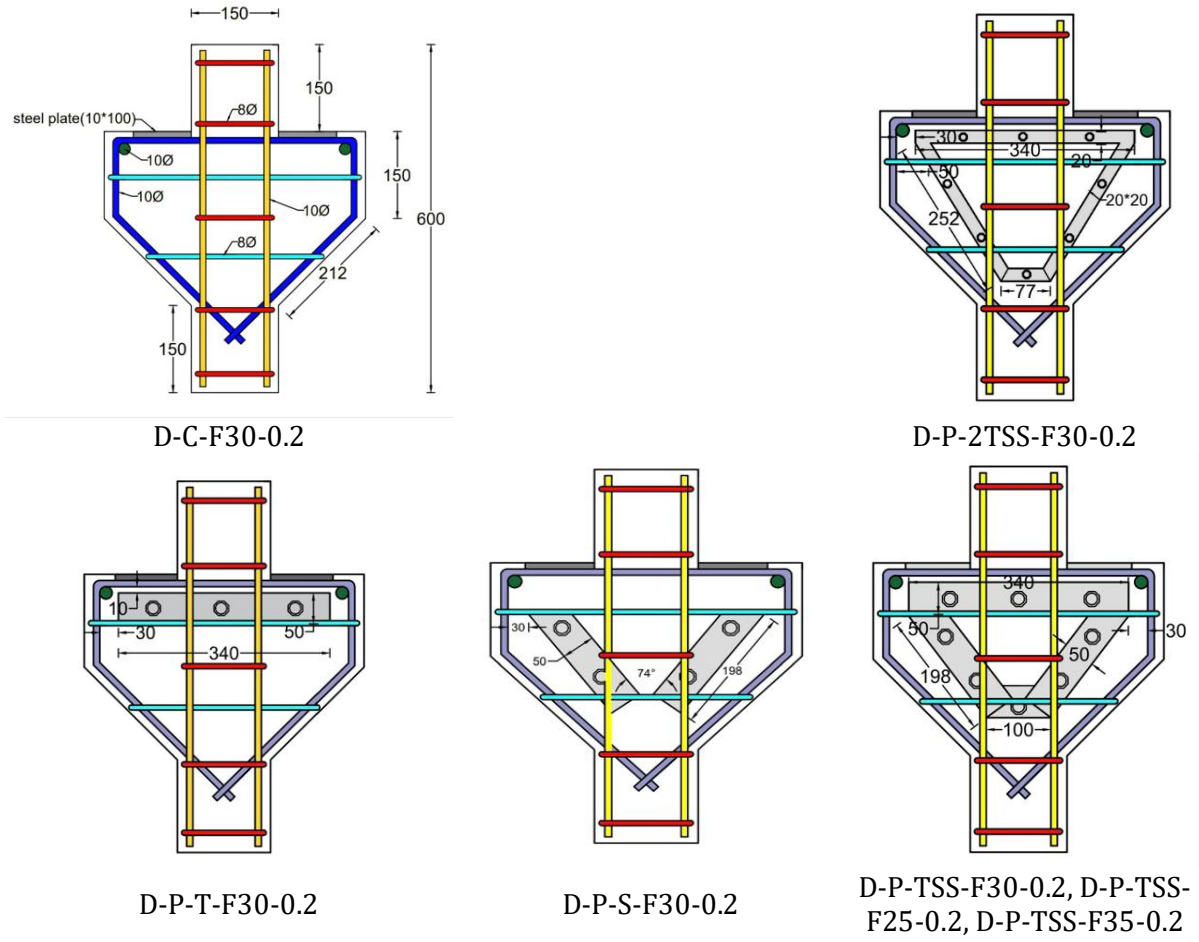


Fig. 1. Details of reinforcement and geometry of the tested corbels

In compliance with Iraqi standards, reverse osmosis (RO) water was utilized to mix and cure the concrete samples. Specification (IQS 1703/2018) [23]. Steel reinforcing bars with deformations of Ø10 mm and Ø8 mm were used. Several steel hollow boxes of varying sizes were employed. The square hollow box has two alternative dimensions (50×50 mm^2 and 20×20 mm^2). The materials complied with ASTM A615/A615M-20 [24] for reinforcement bars and ASTM A370-10 [25] for steel section evaluation. Table 3 presents the characteristics of the reinforcing bars and steel sections. Since the geometry of the tested corbels required non-standard steel configurations, the hollow steel sections (HSS) were fabricated from separate steel pieces that were cut to the required dimensions and subsequently assembled using electric arc welding. The welding electrodes used were J38.12/E6013, with a diameter of 2.5 mm. According to the American Welding Society Standard (AWS D1.1/D1.1M:2020) [26], these electrodes can be used with AC or DC polarity, with a recommended welding current of 50–90 A. The assembled steel components were connected using fillet welds with a nominal weld size of 3 mm, in accordance with ANSI/AISC 360-22 [27]. After welding, the connections were visually inspected to check the general appearance and continuity of the welds and to identify any visible surface defects. Steel bearing plates (150 × 100 × 10 mm) were welded to the primary tension reinforcement. Steel bolts were used as shear

connectors between the hollow steel sections (HSS) and the surrounding concrete. The bolts had a diameter of 9 mm and a total length of 50 mm. The bolts were welded directly to the HSS before concrete casting using electric arc welding. The shear connectors were spaced at 15 cm along the member.

Table 1. Grading of the fine aggregates (sand)

No.	Sieve size(mm)	Percent passing (%)	Iraqi Specification IQS45/1984 for Zone (2)
1	10	100	100
2	4.75	97.8	90-100
3	2.36	88.8	75-100
4	1.18	75.4	55-90
5	0.6	57	35-59
6	0.3	26.6	8-30
7	0.15	3.4	0-10
Materials passing through a sieve of 75 micron (%)		4.2	≤ 5%

Table 2. Coarse aggregate grading

No.	Sieve size (mm)	Percent passing (%)	Iraqi Specification IQS45/1984 for Zone (2)
1	12.5	100	100
2	9.5	100	85-100
3	4.75	10	25-0
4	2.36	1	5-0

Table 3. Average characteristics of steel sections and reinforcing bars

$D_{nominal}$(mm)	Test results	
	Yield strength (N/mm²)	Ultimate strength (N/mm²)
8 mm	338	563
10 mm	650	807
Hollow steel box (20×20)	330	370
Hollow steel box (50×50)	320	375

2.4 Concrete Mix Design

In this study, normal concrete with different compressive strengths was used, in accordance with the mixture proportions described in Table 4.

Table 4. Percentages of the concrete mix

NO	Materials	25 (kg/m^3)	30 (kg/m^3)	35 (kg/m^3)
1	cement	250	412	480
2	water	200	212	183
3	gravel	1100	1064	1082
4	sand	850	656	635

2.5 Fresh Concrete Tests

To check the quality of the concrete mix while casting the major specimens, the workability of the concrete mixes was evaluated using the slump test according to ASTM C143 [28]. The slump values obtained for each mix are presented in Table 5.

Table 5. Results of the slump test

No.	Type of concrete	Slump value (mm)
1	f_c25	100
2	f_c30	100
3	f_c35	90

2.6 Mechanical Properties of Hardened Concrete

The tests on hardened concrete were performed in the laboratory. Three cylinders with dimensions of 100×200 mm were tested in compliance with ASTM C31/C31M-21 to ascertain the concrete's compressive strength [29]. Three prisms with dimensions of 100x100x500 mm were used to measure flexural strength in accordance with ASTM C78-02 [30]. Three cylinders measuring 100×200 mm were utilized for the splitting. Tensile strength test in compliance with ASTM C496-17 [31]. The results of the above tests are shown in Table 6.

Table 6. Results of tests on hardened concrete

Compressive strength f_{cu} (MPa)	Flexural strength (MPa)	Tensile strength f_t (MPa)
25.1	3.2	2.15
29	3.3	2.9
35.5	3.5	3.1

2.7 Test Setup and Instrumentation

Figure 2 shows the test equipment that had a 1000 kN load capacity, which was utilized to test each sample. The machine can regulate and modify the loading rate as necessary. A linear variable differential transformer (LVDT) was positioned beneath the corbel during the loading process to quantify deflection. The specimens were subjected to monotonic loading, with the applied load increased incrementally by 1 kN until failure. No specific holding period was applied between successive load increments. Loading was continued until the specimen reached its ultimate load and exhibited a clear failure condition.



Fig. 2. Testing devices, LVDT, data logger

3. Results and Discussion

Table 7 displays the assessed specimens, specifying the cracking load, ultimate load, maximum deflection, and failure mode. This document provides a detailed explanation of each specimen.

Table 7. Experimental test results of specimens

Specimen	Load (kN)		Max deflection, mm	Mode of failure
	Cracking, Pcr	Ultimate, Pu		
D-C-F30-0.2	100	250	3.5	Shear compression failure
D-P-T-F30-0.2	250	600	3.2	Shear tension failure
D-P-S-F30-0.2	260	631.5	3.8	Shear tension failure
D-P-TSS-F25-0.2	200	396.5	4.2	Shear tension failure
D-P-TSS-F35-0.2	200	595	2.5	Shear compression failure
D-P-2TSS-F30-0.2	230	560	3.2	Shear compression failure
D-P-TSS-F30-0.2	230	538.5	2.5	Shear tension failure

3.1 Failure Modes and Crack Propagation of the Specimens

Figure 3 presents the observed crack propagation and failure modes of the tested corbels. The control specimen, D-C-F30-0.2, developed the first visible crack at 100 kN and failed at 250 kN by shear compression. In contrast, all strengthened specimens developed their first visible cracks at higher load levels, ranging from 200 to 260 kN. Therefore, compared with the control specimen, the first-cracking load increased by 100% to 160% depending on the strengthening configuration. This indicates that the proposed strengthening system delayed the appearance of the first visible cracks. The increase in first-cracking load was accompanied by a substantial increase in ultimate load. The strengthened specimens reached ultimate loads between 396.5 and 631.5 kN, compared with 250 kN for the control specimen, corresponding to increases of 58.6% to 152.6%. The greatest increase was obtained for D-P-S-F30-0.2, with 631.5 kN, while D-P-TSS-F25-0.2 recorded the lowest ultimate load among the strengthened specimens, with 396.5 kN. The results therefore show that the strengthening arrangement had a considerable effect on both crack initiation and ultimate load. A direct comparison of the three specimens strengthened in the tie and strut regions, D-P-TSS-F25-0.2, D-P-2TSS-F30-0.2, and D-P-TSS-F35-0.2, provides a clearer view of the differences in their observed behavior. The first-cracking loads were 200, 230, and 200 kN, respectively, while the ultimate loads were 396.5, 560, and 595 kN. Thus, D-P-2TSS-F30-0.2 showed a 15% higher first-cracking load than both D-P-TSS-F25-0.2 and D-P-TSS-F35-0.2. Its ultimate load was 41.2% higher than that of the 25 MPa specimen but 5.9% lower than that of the 35 MPa specimen.

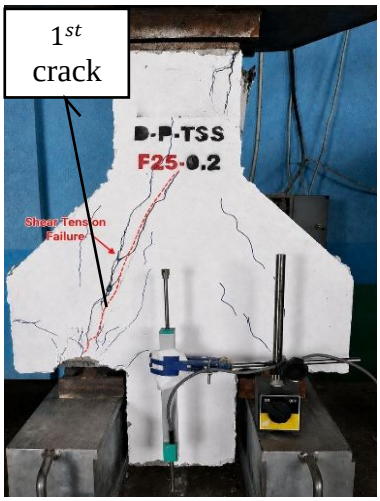
The comparison between D-P-TSS-F25-0.2 and D-P-TSS-F35-0.2 is particularly important because both specimens had the same strengthening arrangement. Increasing the concrete compressive strength from approximately 25 MPa to 35 MPa did not change the first-cracking load, which remained at 200 kN. However, the ultimate load increased from 396.5 to 595 kN, representing an increase of approximately 50.1%. The observed failure mode also changed from shear tension in the 25 MPa specimen to shear compression in the 35 MPa specimen. This difference was observed experimentally and indicates that the two specimens reached failure through different failure modes.

The crack propagation and failure observations also show differences among the strengthening configurations. D-P-T-F30-0.2 and D-P-S-F30-0.2 failed by shear tension, whereas D-P-2TSS-F30-0.2 and D-P-TSS-F35-0.2 failed by shear compression. The control specimen also failed by shear compression, while D-P-TSS-F25-0.2 failed by shear tension. Thus, the observed failure modes were not identical for all strengthened specimens, although shear-related failure was present in all cases.

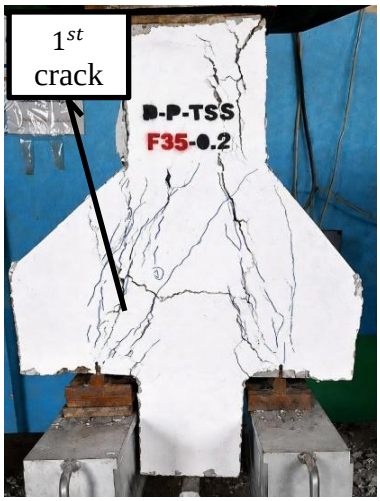
These observations are generally consistent with previous experimental investigations of strengthened RC corbels. Al-Kamaki et al. (2018) reported that strengthening RC corbels with CFRP sheets increased the ultimate load by up to 27% and reduced the development of shear cracks. The present study produced higher increases in ultimate load, ranging from 58.6% to 152.6% compared with the control specimen. The difference in the magnitude of improvement can be attributed to the different strengthening materials and strengthening arrangements investigated

in the two studies. Previous experimental studies have also reported diagonal cracking and shear-related failure as common characteristics of reinforced concrete corbels.

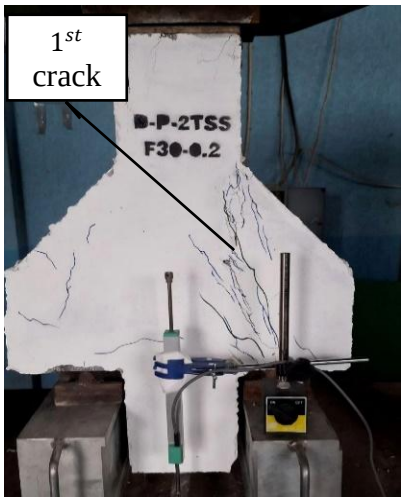
Overall, the experimental results demonstrate that the proposed hollow steel section strengthening system increased both the load required to initiate the first visible crack and the ultimate load.



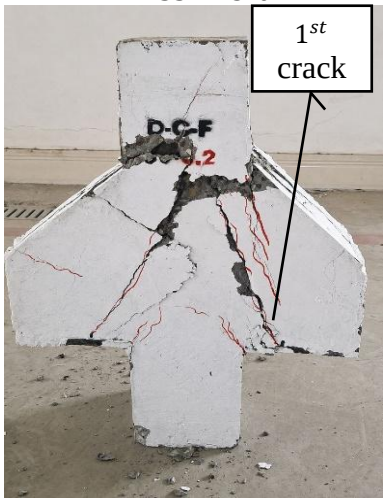
D-P-TSS-F25-0.2



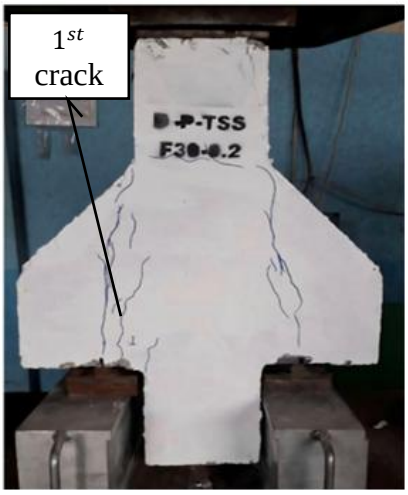
D-P-TSS-F35-0.2



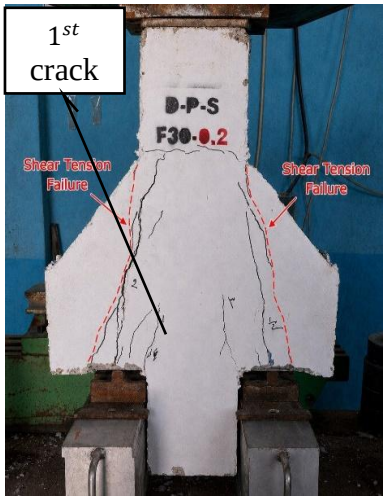
D-P-2TSS-F30-0.2



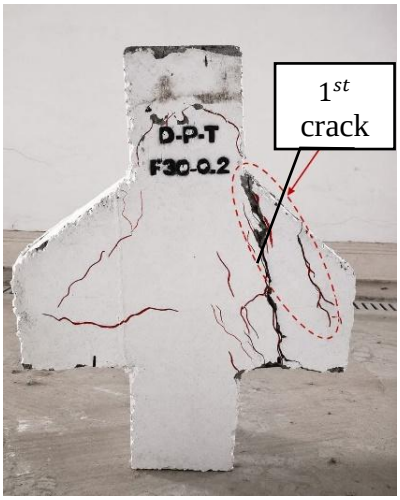
D-C-F30-0.2



D-P-T-F30-0.2



D-P-S-F30-0.2



D-P-TSS-F30-0.2

Fig. 3. Mode of failure of the corbels. Scale = 1:10.5, Scale

3.2 Load-Deflection Curve

Figure 4 presents the load–deflection responses of the tested corbels. The proposed strengthening system significantly increased the ultimate load compared with the control specimen, D-C-F30-0.2, which reached 250 kN at approximately 3.5 mm deflection. The strengthened specimens achieved ultimate loads of 396.5–631.5 kN, corresponding to increases of 58.6–152.6%. For specimens with approximately 30 MPa concrete, D-P-S-F30-0.2 achieved the highest ultimate load of 631.5 kN, followed by D-P-T-F30-0.2 (600 kN), D-P-2TSS-F30-0.2 (560 kN), and D-P-TSS-F30-0.2 (538.5 kN). Notably, D-P-TSS-F30-0.2 achieved 115.4% higher ultimate load than the control while exhibiting a lower maximum deflection of approximately 2.5 mm. The effect of concrete compressive strength was evident in the TSS specimens. Increasing the strength from 25 to 30 MPa and from 30 to 35 MPa increased the ultimate load by 35.8% and 10.5%, respectively, while the overall increase from 25 to 35 MPa was 50.1%. The maximum deflection also decreased from approximately 4.2 to 2.5 mm. Overall, the results indicate that strengthening substantially enhanced load-carrying capacity without a proportional increase in maximum deflection. The strut-strengthened specimen achieved the highest capacity, while the TSS-F30 specimen demonstrated a favorable combination of high load capacity and low deflection. Since stress and strain measurements were not conducted, the observed differences are discussed based solely on the measured load–deflection response.

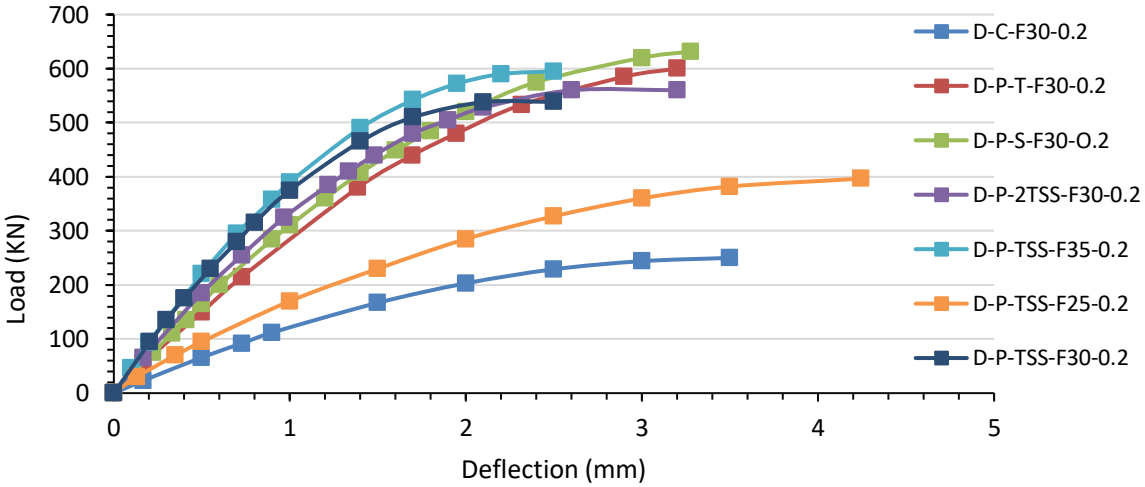


Fig. 4. Load-deflection curves for all investigated specimens

3.3 Stiffness, Toughness, and Ductility

Stiffness (K) measures the resistance to deformation exhibited by an elastic body. The effective secant stiffness, which corresponds to the load stage (0.75Pu), is used for evaluation [32], as represented by Eq. (1).

$$K_{eff} = \frac{0.75_{Pu}}{\Delta_{0.75pu}} \quad (1)$$

Where; K_{eff} : effective stiffness, Pu: ultimate load, $\Delta_{0.75pu}$: deflection value corresponding to the 0.75 Pu load level.

The control specimen, D-C-F30-0.2, recorded a stiffness of 104.16 kN/mm. Compared with the control, the stiffness increased by 146.9% for D-P-T-F30-0.2, 159.8% for D-P-S-F30-0.2, 189.0% for D-P-TSS-F30-0.2, 210.0% for D-P-2TSS-F30-0.2, and 229.5% for D-P-TSS-F35-0.2. In comparison, D-P-TSS-F25-0.2 showed the lowest increase of 35.9%. Among the TSS specimens, stiffness increased from 141.6 kN/mm at 25 MPa to 301 kN/mm at 30 MPa and 343.26 kN/mm at 35 MPa. This indicates that the measured stiffness increased with concrete compressive strength within the TSS group. The area under the load-deflection curve, which represents toughness, is a measure of a member's resistance to deformation before failure [33], as represented by Eq. (2).

$$T = \int_0^{\Delta u} P(\Delta)\, d\Delta \quad (2)$$

Where; T: toughness, P = load(Kn), Δ: The deflection (mm), Δu: The deflection at the ultimate load.

The control specimen recorded a toughness of 581 kN·mm, while the strengthened specimens showed higher values. D-P-S-F30-0.2 achieved the highest toughness of 1338 kN·mm, representing an increase of 130.3% compared with the control. D-P-2TSS-F30-0.2 and D-P-T-F30-0.2 followed with increases of 120.0% and 110.0%, respectively. The toughness values of D-P-TSS-F25-0.2, D-P-TSS-F30-0.2, and D-P-TSS-F35-0.2 were 1124, 1000, and 986 kN·mm, respectively. Thus, within the TSS group, toughness decreased as concrete compressive strength increased. Ductility (μ), which is represented by Eq. (3) [34], is the capacity to withstand inelastic deformation without reducing the ultimate load till failure. Ductility index was calculated as the ratio of the ultimate deflection (Δ_u) to the yield deflection (Δ_y), as shown in Figure 5.

$$\mu = (\Delta_u/\Delta_y) \quad (3)$$

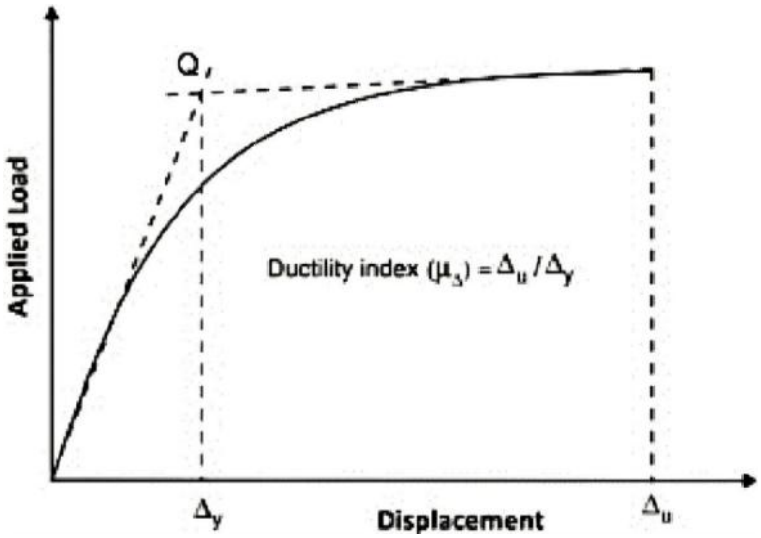


Fig. 5. Calculating the ductility ratio using the displacement ratio method

The control specimen recorded a ductility value of 4.375, compared with 4.57, 4.095, 5.30, 4.4425, 4.00, and 3.201 for D-P-T-F30-0.2, D-P-S-F30-0.2, D-P-TSS-F25-0.2, D-P-TSS-F30-0.2, D-P-TSS-F35-0.2, and D-P-2TSS-F30-0.2, respectively. Compared with the control specimen, D-P-T-F30-0.2 showed a slight increase in ductility of approximately 4.5%, whereas D-P-S-F30-0.2 showed a reduction of approximately 6.4%. D-P-TSS-F30-0.2 remained close to the control, with an increase of approximately 1.5%. The highest ductility was obtained for D-P-TSS-F25-0.2, with a value of 5.30, representing an increase of approximately 21.1% compared with the control. In contrast, D-P-2TSS-F30-0.2 recorded the lowest ductility among the strengthened specimens, with a value of 3.201, representing a reduction of approximately 26.8%. Within the TSS group, ductility decreased from 5.30 at 25 MPa to 4.4425 at 30 MPa and 4.00 at 35 MPa. This represents an overall reduction of approximately 24.5% between the 25 and 35 MPa specimens. Therefore, the increase in concrete compressive strength within the TSS group was accompanied by an increase in stiffness, while toughness and ductility decreased.

Table 8. Outcomes of stiffness, toughness, and ductility for all specimens

No.	Specimens	Stiffness (kN/mm)	Toughness (kN·mm)	Ductility
1	D-C-F30-0.2	104.16	581	4.38
2	D-P-T-F30-0.2	257.14	1220	4.57
3	D-P-S-F30-0.2	270.6	1338	4.1
4	D-P-TSS-F25-0.2	141.6	1124	5.3
5	D-P-TSS-F35-0.2	343.26	986	4
6	D-P-2TSS-F30-0.2	323	1278	3.2
7	D-P-TSS-F30-0.2	301	1000	4.44

4. Conclusions

Based on the experimental investigation of reinforced concrete corbels strengthened using embedded hollow steel sections, the following conclusions can be drawn:

- The proposed hollow steel section strengthening system significantly increased the first-cracking load and ultimate load of the tested corbels compared with the control specimen. The first-cracking load increased from 100 kN for the control specimen to 200–260 kN for the strengthened specimens, corresponding to increases of 100%–160%. The ultimate load increased from 250 kN to 396.5–631.5 kN, representing improvements of 58.6%–152.6%.
- The strengthening configuration had a clear influence on the load-carrying capacity. Among the specimens with approximately 30 MPa concrete and an a/d ratio of 0.2, D-P-S-F30-0.2 achieved the highest ultimate load of 631.5 kN, followed by D-P-T-F30-0.2 at 600 kN, D-P-2TSS-F30-0.2 at 560 kN, and D-P-TSS-F30-0.2 at 538.5 kN.
- Increasing the concrete compressive strength within the TSS strengthening configuration increased the ultimate load from 396.5 kN at approximately 25 MPa to 595 kN at approximately 35 MPa, representing an overall increase of 50.1%. However, the first-cracking load remained 200 kN for both specimens.
- The observed failure modes varied among the tested specimens. The control specimen and the D-P-2TSS-F30-0.2 and D-P-TSS-F35-0.2 specimens exhibited shear compression failure, whereas D-P-T-F30-0.2, D-P-S-F30-0.2, and D-P-TSS-F25-0.2 exhibited shear tension failure.
- The measured effective secant stiffness increased for all strengthened specimens relative to the control. Within the TSS group, stiffness increased from 141.6 kN/mm at approximately 25 MPa to 343.26 kN/mm at approximately 35 MPa.
- All strengthened specimens exhibited higher toughness than the control specimen. The highest toughness was recorded for D-P-S-F30-0.2 at 1338 kN·mm, compared with 581 kN·mm for the control specimen.
- The ductility response varied with the strengthening configuration and concrete compressive strength. D-P-TSS-F25-0.2 exhibited the highest ductility index of 5.30, while D-P-2TSS-F30-0.2 exhibited the lowest value of 3.201. Within the TSS group, increasing concrete compressive strength was accompanied by increased stiffness but reduced toughness and ductility.

References

[1] American Concrete Institute. 318-19 Building code requirements for structural concrete and commentary. 2019.
[2] Mattock AH, Chen KC, Soongswang K. The behavior of reinforced concrete corbels. PCI Journal. 1976;21(2):52-77. https://doi.org/10.15554/pcij.03011976.52.77
[3] Shakir QM. Performance assessment of high strength concrete two-sided corbels with embedded stiffened web-rolled steel. Structures. 2021;32:1469-1480. https://doi.org/10.1016/j.istruc.2021.03.098
[4] Shakir QM, Abdlsaheb SD. Rehabilitation of partially damaged high strength RC corbels by EB FRP composites and NSM steel bars. Structures. 2022;38:652-671. https://doi.org/10.1016/j.istruc.2022.02.023
[5] Torres FM. Theoretic-experimental analysis of reinforced concrete corbels [Master's thesis]. São Carlos: Engineering School of São Carlos, São Paulo University; 1998.
[6] Shakir QM. Behavior of high-performance RC composite corbels with inclined stirrups. Canadian Journal of Civil Engineering. 2022;49:18-30. https://doi.org/10.1139/cjce-2020-0149
[7] Shakir QM, Abdlsaheb SD. Strengthening of the self-compacted reinforced concrete corbels using NSM steel bars and CFRP sheets techniques. J Eng Sci Technol. 2022;17(3):1764-1780.
[8] Neupane RC, Eddy L, Nagai K. Investigation on strengthening approaches adopted for poorly detailed RC corbels. Fibers. 2017;5(2):16. https://doi.org/10.3390/fib5020016
[9] de Souza RA, Trautwein LM, Ferreira M de P. Reinforced concrete corbel strengthened using carbon fiber reinforced polymer (CFRP) sheets. Journal of Composites Science. 2019;3(1):26. https://doi.org/10.3390/jcs3010026
[10] Heidayet A, Ramadhan A, Qarani O. Repairing of damaged reinforced concrete corbels strengthened by externally bonded steel plates. Zanco Journal of Pure and Applied Sciences. 2004;16(1).
[11] Ozden S, Atalay HM. Strengthening of reinforced concrete corbels with GFRP overlays. Science and Engineering of Composite Materials. 2011;18:69-77. https://doi.org/10.1515/secm.2011.009

[12] El-Maaddawy TA, Sherif E-SI. Response of concrete corbels reinforced with internal steel rebars and external composite sheets: Experimental testing and finite element modeling. Journal of Composites for Construction. 2014;18(2). https://doi.org/10.1061/(ASCE)CC.1943-5614.0000403
[13] Mohammed AA, Hassan GB. Load capacity and deformation of high-strength concrete corbels wrapped with CFRP sheets. In: The 2nd International Conference of Buildings, Construction and Environmental Engineering (BCEE2-2015); 2015.
[14] Ivanova I, Assih J. Experimental study of local behavior of strengthened reinforced concrete short corbel by bonding carbon fiber fabrics. International Journal of Structural and Civil Engineering Research. 2015.
[15] Ivanova I, Assih J. Static and dynamic experimental study of a strengthened reinforced short concrete corbel using carbon fabrics, crack path in the shear zone. Frattura ed Integrità Strutturale. 2015;34:90-98. https://doi.org/10.3221/IGF-ESIS.34.09
[16] Urban T, Krawczyk Ł, Gołdyn M. Strengthening of short reinforcement concrete corbel using steel accessory. Unpublished manuscript or report; n.d.
[17] Mohammad AKQ, Al-Shamaa MFK. Experimental study of behaviour of reactive powder concrete strengthening by NSM-CFRP corbels. Civil Engineering Journal. 2018;4:980-992. https://doi.org/10.28991/cej-0309150
[18] Al-Kamaki YSS, Hassan GB, Alsofi G. Experimental study of the behaviour of RC corbels strengthened with CFRP sheets. Case Studies in Construction Materials. 2018;9:e00181. https://doi.org/10.1016/j.cscm.2018.e00181
[19] Shakir QM, Kamonna HHH. The behavior of high strength self-compacting reinforced concrete corbels strengthened with NSM steel bars. International Journal of Advanced Science, Engineering and Information Technology. 2018;8:1022-1028. https://doi.org/10.18517/ijaseit.8.4.5905
[20] Braidi WI, Mohsin RD, Tu'ma NH, Raheem HAK. Experimental investigation of eccentric composite hollow steel-concrete tensioned column. Civil and Environmental Engineering. 2026. https://doi.org/10.2478/cee-2026-0061
[21] Central Organization for Standardization and Quality Control, Iraq. Iraqi specifications 5/2019: Portland Cement [In Arabic]. 2019.
[22] Central Organization for Standardization and Quality Control, Iraq. Iraqi Specification No. 45: Natural sources for gravel that is used in concrete and construction. Baghdad; 1984.
[23] Central Organization for Standardization and Quality Control, Iraq. Iraqi specifications 1703/2018: Water used for concrete [In Arabic]. 2018.
[24] ASTM International. Standard specification for deformed and plain carbon-steel bars for concrete reinforcement (ASTM A615/A615M-20). 2020.
[25] ASTM International. Standard test method and definition for mechanical testing of steel products (ASTM A370-10). In: Annual Book of ASTM Standards, Vol. 01.01. Philadelphia, PA: ASTM; 2005.
[26] American Welding Society. Structural welding code-Steel. Mar Lin; 2020.
[27] American Institute of Steel Construction (AISC). Specification for Structural Steel Buildings (ANSI/AISC 360-22). Chicago, IL: AISC; 2022.
[28] ASTM International. Standard test method for slump of hydraulic-cement concrete (ASTM C143-17). 2017.
[29] ASTM International. Standard practice for making and curing concrete test specimens in the field (ASTM C31/C31M-21a). 2021.
[30] ASTM International. Standard test method for flexural strength of concrete (using simple beam with third-point loading) (ASTM C78-09). 2009.
[31] ASTM International. Standard test method for splitting tensile strength of cylindrical concrete specimens (ASTM C496/C496M-17). 2017.
[32] Park R. Ductility evaluation from laboratory and analytical testing. In: Proceedings of the 9th World Conference on Earthquake Engineering, Vol. 8. Tokyo-Kyoto, Japan; 1988. p. 605-616.
[33] Shakir QM, Abd BB. Retrofitting of self-compacting RC half joints with internal deficiencies by CFRP fabrics. Jurnal Teknologi (Sciences and Engineering). 2020;82(6):49-62. https://doi.org/10.11113/jurnalteknologi.v82.14416
[34] Naaman A, Jeong M. Structural ductility of concrete beams prestressed with FRP tendons. In: Non-Metallic (FRP) Reinforcement for Concrete Structures: Proceedings of the Second International RILEM Symposium. Boca Raton, FL, USA: CRC Press; 1995. p. 379.